

Towards a highly performing lithium-metal battery with glyme solution and olivine cathode

Shuangying Wei^a, Shoichi Inoue^b, Dr. Daniele Di Lecce^a, Dr. Zhenguang Li^b, Prof. Dr. Yoichi Tominaga^{b,c,*}, Prof. Dr. Jusef Hassoun^{a,c,d,*}

^a *University of Ferrara, Department of Chemical and Pharmaceutical Sciences, Via Fossato di Mortara 17, 44121, Ferrara, Italy.*

^b *Tokyo University of Agriculture and Technology (TUAT), Graduate School of Bio-Applications and Systems Engineering (BASE), 2-24-16, Naka-cho, Koganei-shi, Tokyo 184-8588, Japan.*

^c *Institute of Global Innovation Research (GIR), Tokyo University of Agriculture and Technology (TUAT), Tokyo, Japan*

^d *National Interuniversity Consortium of Materials Science and Technology (INSTM) University of Ferrara Research Unit, University of Ferrara, Via Fossato di Mortara, 17, 44121, Ferrara, Italy.*

Corresponding Authors: jusef.hassoun@unife.it, ytominag@cc.tuat.ac.jp

Abstract

High-performance lithium-metal battery is herein achieved by using a glyme-based electrolyte enhanced with LiNO₃ additive and LiFePO₄ cathode. An optimal electrolyte formulation is selected upon detailed analysis of the electrochemical properties of various solutions formed by dissolving respectively lithium bis(fluorosulfonyl)imide (LiFSI), lithium bis(trifluoromethanesulfonyl)imide (LiTFSI), and lithium bis(pentafluoroethanesulfonyl)imide (LiBETI) either in diethylene glycol dimethyl ether or in triethylene glycol dimethyl ether and by adding LiNO₃. A thorough investigation evidences efficient ionic transport, wide stability window, low reactivity with lithium metal, and cathode/electrolyte interphase characteristics strongly depending on the glyme chain length. The best Li/LiFePO₄ battery delivers 154 mAh g⁻¹ at C/3 (1C = 170 mA g⁻¹) without any decay after 200 cycles. Tests within 1C and 5C show initial capacities of about 150 and 140 mAh g⁻¹, a retention exceeding 70% after 500 cycles, and suitable electrode/electrolyte interphases evolution.

Keywords

Glyme electrolyte; LiNO₃; salt effect; electrochemistry; lithium metal.

Introduction

Lithium-ion batteries are currently diffused in portable electronics, including laptops, digital cameras, smartphones, and actually proposed for electric vehicles, owing to suitable gravimetric and volumetric energy densities (up to 250 Wh kg⁻¹ and 650 Wh l⁻¹) as well as long lifespan.^[1,2] The typical Li-ion cell configuration is based on insertion/intercalation electrodes, e.g., layered or olivine-structure cathode and graphite anode, which ensure a reasonable safety level despite the use of flammable electrolytes formed by alkyl-carbonate solvents and LiPF₆.^[3] Although the remarkable performances demonstrated by the graphite-based anodes in conventional rechargeable cells,^[4] a renewed interest is now devoted towards the lithium-metal electrode,^[5,6] which is presently limited to primary configurations and polymer secondary batteries due to risks of possible thermal runaways upon cycling into the typical configuration.^[7,8]

The lithium-metal electrode has a theoretical specific capacity as high as 3860 mAh g⁻¹ (vs. 372 mAh g⁻¹ for graphite), the lowest electrochemical potential (3.040 V vs. SHE compared to 2.84 V vs. SHE for graphite) and a density of 0.59 g cm⁻³ (vs. 2.25 g cm⁻³ for graphite).^[9] Accordingly, lithium-metal batteries with ultrahigh energy densities, including Li-sulfur^[10,11] and Li-air cells,^[12,13] have become a popular research topic. Analogously to graphite, meanwhile with different features and magnitude, the lithium metal anode is thermodynamically unstable in most electrolyte solutions, thereby requiring an adequate solid electrolyte interphase (SEI) layer to kinetically prevent parasitic reactions which affect anode, electrolyte and cycling performance,^[14] and possibly limit hazardous dendritic growth.^[6,15] Therefore, an improved lithium/electrolyte interphase is crucial for ensuring at the same time fast charge transfer and electrochemical stability upon long-term cycling.^[14] Moreover, the high reactivity of lithium metal requires *ad hoc* solutions with lower flammability than conventional electrolytes.^[16]

Recent studies have been attempting to solve the intrinsic issues associated with the use of lithium metal by focusing on gel/solid polymer electrolytes or inorganic solid electrolytes usually ensuring satisfactory charge transport properties at medium-high temperature, which may limit practical applications.^[17-21] As for the liquid electrolyte solutions, poly(ethylene glycol) dimethyl ethers with general formula $R_1O(CH_2CH_2O)_nR_2$ (where R_1 and R_2 are alkyl groups), also called end-capped glymes, have been investigated as possible solvents for various lithium salts, such as those employing the bis(fluorosulfonyl)imide (FSI⁻),^[22] bis(trifluoromethanesulfonyl)imide (TFSI⁻),^[23] bis(pentafluoroethanesulfonyl)imide (BETI⁻),^[24] and trifluoromethanesulfonate ($CF_3SO_3^-$) anions.^[25] Glyme-based electrolytes have demonstrated suitable Li^+ transport and adequate electrochemical stability window for battery application, higher flash point than carbonate-based and 1,3-dioxolane/dimethyl ether-based solutions,^[26] as well as tunable chemical and physical properties that by changing the chain length.^[27-30] Furthermore, the use of suitable additives remarkably enhanced the electrode passivation behavior,^[31,32] leading to promising cell performances. Indeed, literature works have shown that vinylene carbonate (VC),^[33,34] fluoroethylene carbonate (FEC),^[35,36] and lithium nitrate ($LiNO_3$)^[37,38] may improve the SEI between anode and electrolyte. In particular, it is widely demonstrated that $LiNO_3$ -containing electrolytes may form a uniform and stable anode passivation layer containing both organic (*i.e.*, $ROLi$ and $ROCO_2Li$) and inorganic (*i.e.*, Li_xNO_y , Li_3N , and Li_2O) species, which can mitigate the parasitic reactions in the cell and limit the lithium dendrite growth.^[39-42] Hence, $LiNO_3$ has been extensively studied in Li-S cells as lithium protective agent able to prevent the chemical reduction at the anode side of the long-chain polysulfides (Li_2S_x , $4 \leq x \leq 8$).^[43] Moreover, recent works suggested a beneficial effects of $LiNO_3$ in cells using electrolyte solutions of triethylene, tetraethylene, and polyethylene glycol dimethyl ethers with $LiCF_3SO_3$ and olivine cathodes.^[31,32,44] Following this trend, we have lately investigated the electrochemical characteristics of various electrolyte formulations employing diethylene glycol dimethyl ether ($((CH_3OCH_2CH_2)_2O$, DEGDME) and triethylene glycol dimethyl ether ($CH_3(OCH_2CH_2)_3OCH_3$, TREGDME) with LiFSI, LiTFSI and LiBETI, which demonstrated promising characteristics for

application in lithium cells using LiFePO_4 .^[45] Herein we explore the effect of the addition of LiNO_3 to the above electrolytes in terms of cell performances and, in particular, in terms of cycle life and electrode/electrolyte interphase stability. We investigate accordingly six LiNO_3 -containing solutions respectively formed by dissolving LiFSI, LiTFSI, and LiBETI in DEGDME and TREGDME. Ionic conductivity and Li^+ transference number, electrochemical stability window, as well as lithium/electrolyte interphase are studied by means of impedance spectroscopy, chronoamperometry, voltammetry and galvanostatic cycling techniques. In particular, the work sheds light on the different characteristics of the various compositions for a possible application in Li/LiFePO₄ batteries with expected enhanced safety compared to the lithium cells using conventional ethylene carbonate/dimethyl carbonate (EC/DME) solutions.^[26,44] The cathode/electrolyte interphase behavior during galvanostatic charge/discharge over 200 cycles is further investigated by *ex situ* X-ray diffraction and electron microscopy. Hence, we employ the most optimized formulation over 500 charge/discharge cycles and explore the cell resistance and its coulombic efficiency, and propose the use of LiNO_3 -containing, glyme-based electrolytes as an effective strategy to enable rechargeable lithium-metal batteries.

Results and Discussion

Full electrochemical investigation is performed on the electrolytes prior to the use in lithium battery. Figure 1 reports a summary of the main electrochemical characteristics of the solutions,^[46] namely the charge transport properties (panel a), the electrochemical stability window (panel b), the stability against the lithium-metal under both static and dynamic conditions as described by the interphase resistance trend upon cell aging (panel c), and the electro-deposition/dissolution overvoltage upon cycling (panel d). In detail, the charge transport ability has been evaluated by coupling ionic conductivity (Figure 1a, main panel) and lithium transference number (t^+ , Figure 1a, panel inset) measurements. Chronoamperometry profiles and Nyquist plots employed for t^+ calculation are displayed Figure S1 in the Supporting Information (see the experimental section and Table S1 for

further details).^[47] The electrolytes display an ionic conductivity ranging from 10^{-3} to 10^{-2} S cm⁻¹ within the temperature window from 0 to 80 °C, that is, a promising response for possible application in lithium batteries.^[46] Based on the literature,^[25,48–50] the temperature dependence of the ionic conductivity of glyme-based solutions may follow either an Arrhenius or a Vogel–Tamman–Fulcher (VTF) trend, according to the investigated temperature range along with the electrolyte formulation in terms of chemical composition and lithium salt concentration. Herein, the conductivity values may be interpolated by the VTF equation (see Figure 1a) with squared correlation factors (R^2) higher than 0.99. The estimated t^+ values, ranging from 0.62 ± 0.06 (electrolyte E) to 0.74 ± 0.07 (electrolyte B), suggest high mobility for the lithium ions of all the investigated solutions. Previous works have suggested that large anions with reduced mobility and high charge delocalization, as well as ceramic additive with suitable morphology, porosity and surface chemistry, may facilitate the cation motion in glyme-based electrolytes, while possible specific ionic association may increase the lithium transference number above 0.5.^[51,52] Herein, we observe an opposite t^+ trend as the anion increases for the diglyme- and triglyme-based electrolytes, namely a decrease of t^+ for the former and an increase of t^+ for the latter (see Figure 1a inset as well as Figure S1 and Table S1 in Supporting Information). The change of the cation transference number by varying the anion size may imply complex interactions between the electrolyte components due to the presence of various electron-rich sites able to coordinate Li⁺.^[53] However, it is worth mentioning that significant differences may be observed between the t^+ values evaluated by different approaches, such the potentiostatic polarization measurement (employed herein),^[47] the galvanostatic polarization technique,^[54] the electromotive force method^[55] and the pulse-field gradient NMR (PFG-NMR).^[25] Such discrepancies may be reasonably attributed to the specific assumptions and experimental conditions of the various methods.^[56] Thus, the electrochemical techniques measure the net Li⁺ motion, whereas the PFG-NMR considers the ionic self-diffusion coefficients including the contribution of ionic couples and aggregates which are not involved in the current flow upon polarization.^[55] Notably, previous reports^[57,58] have evidenced possible issues in the experimental determination of I_0 , as the first

available measured current might be different from the actual value reflecting the absence of a concentration gradient within the electrolyte. Accordingly, considering the initial Ohmic current determined by EIS rather than the measured one might lead to significantly lower estimation of the cation transference number values, that is, within the range from 0.33 ± 0.03 and 0.45 ± 0.05 , as described in Supporting Information. Furthermore, the relatively high estimated error on t^+ evaluated by electrochemical method, *i.e.*, about 10%, does not allow us to clearly appreciate significant effects of the electrolyte formulation on the cation transport ability. On the other hand, the results of Figure 1a may be directly compared with our previous reports on analogue electrolyte solutions without LiNO_3 ,^[45] thereby providing an insight on the effect of the formulation on the ion transport. Therefore, electrolyte B shows the best characteristics in terms of ionic conductivity (within the range from 6×10^{-3} to $8 \times 10^{-3} \text{ S cm}^{-1}$) and a Li^+ transference number (*i.e.*, 0.74 ± 0.07). Furthermore, when compared with the LiNO_3 -free counterparts^[45] the diglyme-based electrolytes (A, B, and C) have slightly lower conductivity, while the triglyme-based ones (D, E, and F) exhibit higher values. In this respect, we have shown in a recent work that the LiNO_3 addition to glyme-based solutions may slightly affect the ionic conductivity partly due to changes of viscosity for increasing salt-to-solvent ratios.^[31]

The electrochemical stability window of each electrolyte solution has been determined by linear sweep voltammetry (LSV) and cyclic voltammetry (CV) on two different cells in the high and low voltage regions, respectively (see Figure 1b). Herein, we have used working electrodes formed by mixing conductive agent and binder (see the experimental section for further details about the electrode preparation procedure), which well reproduce the electrolyte behavior on composite cathodes. Indeed, the use of inert metallic electrodes, such as Ni or Pt, might affect the evaluation of the actual applicability of the solutions in practical cells.^[21,31] The experimental data of Figure 1b indicate a current flow lower than $30 \mu\text{A cm}^{-2}$ at 4.3 V *vs.* Li^+/Li for all the electrolyte and suggest their possible use in lithium cell with LiFePO_4 operating at 3.45 V.^[59,60] Furthermore, the figure inset suggests higher oxidative stability for electrolytes B and E, *i.e.*, using the LiTFSI salts, that fully

decompose at potential as high as 4.5 V vs. Li⁺/Li. Based on the existing literature,^[61–66] Al corrosion via dissolution into the electrolyte above 3.5 V vs. Li⁺/Li cannot be excluded. Herein, very weak peaks (the current flow is below 20 μA cm⁻²) are observed between 3.5 and 4.1 V vs. Li⁺/Li, thereby suggesting that the current collector is relatively stable in the solutions within the potential window of LiFePO₄ (LFP). In this regard, a recent work^[31] on a glyme-based electrolyte using LiCF₃SO₃ has shown that LiNO₃ may improve the cathode/electrolyte interphase through decomposition reactions occurring at about 3.8 V vs. Li⁺/Li upon charge and at about 1.5 V vs. Li⁺/Li upon discharge, which lead to precipitation of a passivation layer as revealed by scanning electron microscopy (SEM, see below). As for the low-voltage region, the first cathodic CV scan shows the expected electro-reduction of LiNO₃ which contributes to the SEI formation^[31,32] occurring by a strong current signal between 1.7 and 1.4 V vs. Li⁺/Li. It is worth mentioning that this experimental evidence has not been observed in comparable solution without additive.^[45] In detail, Figure 1b inset reveals voltammetry peaks at about 1.45, 1.52 and 1.57 V vs. Li⁺/Li for electrolytes A, B and C, *i.e.* using diglyme, and at about 1.49, 1.47 and 1.47 V vs. Li⁺/Li for electrolytes D, E and F, *i.e.* using triglyme. Additional electrolyte reduction likely affecting the SEI composition^[45] is observed at lower voltage along with Li⁺ insertion into the carbon electrode and lithium plating^[67] which are partially reversible upon the subsequent oxidation scan.

As mentioned in the introduction, a stable interphase between lithium and electrolyte can limit undesired parasitic reaction during cycling^[14] and mitigate the lithium dendrite growth.^[6,15] Herein, electrochemical impedance spectroscopy (EIS) experiments on symmetrical Li/Li cells aged for 31 days may help us to assess the chemical stability of the SEI formed by chemical reaction of the electrolyte species over the lithium-metal electrode by monitoring the related resistance (R_i, see Figure 1c). A detailed analysis of the impedance spectra is reported in the Supporting Information (see Figure S2 and Table S2 for the Nyquist plots and the resistance values, respectively). Figure 1c indicates a relatively stable trend with R_i values lower than 45 Ω (*i.e.*, about 30 Ω cm⁻²) over 1 month of storage. The diglyme-based electrolytes exhibit initial SEI resistances of about 29.1±0.1 Ω (A),

27.7±0.1 Ω (B) and 22.9±0.1 Ω (C), which slightly vary during the first day. Afterwards the R_i values rise to 31.9±0.2 Ω (A), 27.7±0.1 Ω (B) and 35.7±0.2 Ω (C) after 9 days and maintain a stable trend upon 31 days of cell storage with only a minor increase. On the other hand, the triglyme-based solutions show initial resistances of 40.6±0.1 Ω (D), 27.7±0.07 Ω and (E) 25.9±0.09 Ω (F). As for electrolyte D, R_i drops to about 34.1±0.1 Ω after 3 days, then slowly increases to 38.0±0.1 Ω after 9 days and to 42.6±0.1 Ω after 30 days, while electrolyte F exhibits values constantly rising up to 38 Ω after 20 days. Besides, electrolyte E shows an initial increase to about 31 Ω throughout the first 7 days followed by stabilization and slight fluctuation. Therefore, Figure 1c shows a similar decreasing trend of R_i during the first days for electrolytes A and D, *i.e.*, the solutions containing LiFSI, followed by a slight increase. In this respect, previous works have evidenced that the anion properties may affect the chemical composition of the SEI layer over the lithium metal.^[68] Indeed, both anion and solvent promote the lithium passivation via decomposition followed by precipitation of inorganic and organic species containing various species, such as ROLi, RCO₂Li, –CF and –CS moieties, LiF, Li₂O and Li₂CO₃.^[41,69,70] However, we would like to point out that R_i in Figure 1c fluctuates during cell aging in a relatively narrow range (about 10 Ω) for all the investigated formulations, leading to maximum values below 45 Ω which suggest a full compatibility with the lithium-metal anode. Therefore, the electrolytes ensure a rather similar impedance response of the SEI in terms of resistance magnitude despite the expected difference in composition due to the formulation.^[41,69,70] We remark that LiNO₃ leads to a significant improvement of the SEI according to the well-known beneficial effects described in literature,^[31,71] as clearly indicated by a comparison of the data of Figure 1c with previous results on similar electrolytes without additive.^[45] The study under dynamic condition (Figure 1d) further elucidates the stability of the solutions and their compatibility with the lithium-metal battery,^[25] as evidenced by low overvoltage values (below 10 mV for electrolyte A, and below 13 mV for all the other electrolytes) upon 25 days of charge/discharge cycling of symmetrical lithium cells. Again, the data reveals a significant improvement compared with the LiNO₃-free electrolytes,^[45] further demonstrating the crucial role of the additive as stabilizing agent to enhance

the lithium-cell performances. However, Figure 1 avoids clear indication of one of the solutions as the preferred for use in lithium cell; instead it shows possible efficient use of all the electrolytes and suggests further battery measurements for the various samples.

Figure 1

Therefore, the electrochemical behavior of the solutions is additionally evaluated by assembling and cycling at a constant current of C/3 rate Li/LiFePO₄ batteries (1C = 170 mA g⁻¹). Figure 2 reports the results related to the cells using the diglyme-based electrolytes (see panels a-b, c-d, and e-f for electrolytes A, B, and C, respectively) in terms of voltage profiles (panels a, c, e) and trends of capacity and coulombic efficiency (panels b, d, f). The voltage curves reveal the typical flat plateau of LFP centered in 3.5 V^[59] with negligible irreversible capacity after formation of adequate electrode/electrolyte interphases and possible structural rearrangements in the cathode upon the 1st cycle.^[72] The cell using electrolyte A shows an initial polarization of about 160 mV, which gradually increases to 220 mV throughout the measurement (see Figure 2a). It is worth noting that the final segment of the charge/discharge curves at the 150th and 200th cycles show a sloping profile of a diffusion-limited process,^[73] thereby suggesting a possible deterioration of the electrode/electrolyte interphases. Such change of the voltage profile after 100 cycles (see panel a) adversely affects the energy efficiency and leads to a slight capacity fading from about 155 mAh g⁻¹ at the 100th cycle to 144 mAh g⁻¹ at the 200th cycle despite coulombic efficiency values above 99% (see panel b). The cells employing electrolytes B and C exhibit a similar galvanostatic response, while slightly more pronounced capacity fading (see panels c-f). Thus, a gradual interphase deterioration affecting the final segment of the profiles is observed in both cells from the 100th cycle (see panels c and e) in spite of lower polarization values (140 mV for electrolyte B and 130 mV increasing to 170 mV for electrolyte C). The cells deliver reversible capacities of 155 (B, panel d) and 156 mAh g⁻¹ (C, panel f) which decrease to 152 and 154 mAh g⁻¹ after 100 cycles, and to 133 and 135 mAh g⁻¹ after 200 cycles, respectively. As observed for electrolyte A, panels d and f of Figure 2 show coulombic efficiency values permanently above 99% after an initial stabilization during the initial cycles. It is

worth mentioning that the performances of the cells using the diglyme-based electrolytes cannot be completely justified by the electrolyte characteristics observed in Figure 1 and, in particular, by the good lithium-passivation properties of the solutions (see Figure c and d).

Figure 2

Interestingly, the increase of the glyme chain-length from DEGDME to TREGDME ensures a significant enhancement of the electrolyte behavior in the cell with the same amount of LiNO_3 (0.4 mol kg^{-1} , see Figure 3 and the experimental section for further details about the sample composition). The remarkable effect of the solvent allows for the TREGDME-based cells stable voltage profiles which overlap during cycling without any clear sign of degradation of the electrode/electrolyte interphases (see panels a, c, and e of Figure 3 for electrolytes D, E, and F, respectively). Accordingly, the flat curves reflect the signature of the biphasic electrochemical process of LiFePO_4 ,^[74] characterized by a constant voltage during charge and discharge with low polarization ranging from 140 to 170 mV, only slightly increasing after 200 cycles, which suggests fast charge transfer and outstanding cell stability. The batteries deliver reversible capacities of 153 (electrolyte D) and 154 mAh g^{-1} (electrolyte E and F) after an activation during the first 5 cycles,^[72] without any decay over 200 cycles, and a coulombic efficiency permanently within the range from 99.6 to 99.8% (see panels b, d, and f for electrolytes D, E, and F, respectively). As already mentioned, the cycling data may be directly compared with our recent results on the additive-free glyme-based solutions,^[45] which indicated promising electrochemical performances with slight capacity fading from about 150 mAh g^{-1} for the electrolytes using LiTFSI in combination with both the diglyme and the triglyme. On the other hand, the work suggested lower capacity for the other formulations, that is, from 134 to 144 mAh g^{-1} , and a relevant cell failure for the LiBETI-DEGDME solution after about 50 cycles.^[45] Therefore, the addition of LiNO_3 to the electrolytes adopted in this work can affectively enhance the cell behavior due to beneficial electrode-passivation properties^[31,41] leading to remarkable cell stability. However, we remark that further work on the optimization of the LiNO_3 concentration is certainly needed to address the capacity fading issue occurring in diglyme-based cells after about 100

cycles. Instead, the triglyme-based electrolytes with the present formulation exhibit excellent compatibility with the electrode components, as indeed demonstrated by outstanding cycling performances over 200 cycles. In particular, electrolyte E, *i.e.* using LiTFSI, shows the lowest lithium/electrolyte interphase resistance according to Figure 1c and the widest oxidative window according to Figure 1b.

Figure 3

In summary, all the electrolyte solutions have suitable characteristics in terms of ion transport, electrochemical stability window and reactivity against the lithium metal (see Figure 1), which lead to encouraging results with LFP cathode. All the cells of Figures 2 and 3 exhibit the typical flat voltage plateau indicating a Li^+ (de)insertion in a biphasic regime before the 100th cycle (see the related panels a, c, and e).^[74] On the other hand, the voltage curves of the subsequent cycles reveal that the cell response is mostly affected by the glyme solvent rather than by the salt, thereby suggesting a possible effect of the ether-chain length on the passivation layer over the positive and negative electrodes. Thus, the DEGDME-containing cells show two main domains in the voltage plateau after the 100th cycle, namely (i) an initial biphasic regime characterized by a rather constant voltage (initial section of charge and discharge) and (ii) a final regime presenting a sloping curve (final section of charge and discharge), while the TREGDME-containing ones permanently exhibit mainly the typical two-phase response (compare Figure 2a, b and c with Figure 3a, b, and c). The final domain of Figure 2a, b, and c might indicate a Li^+ (de)insertion in the olivine cathode by single-phase, diffusion-limited kinetics,^[75] as observed in LiFePO_4 nanomaterials.^[74] However, a possible increase of the cell resistance due to an excessive growth of the passivation layers on anode and cathode during cycling, likewise leading to a loss of lithium ion concentration in the electrolyte, cannot be excluded.^[73] Furthermore, a sloping profile may arise from a gradual microstructural reorganization occurring in the cathode during cycling in terms of crystallite size distribution and surface free energies of the lithiated and the delithiated phases, possibly leading to a change of the biphasic potential, rather than a different insertion mechanism.^[76] In this respect, a full elucidation of

the observed cell responses is not straightforward. Therefore, we have performed additional EIS measurements on the positive and negative electrodes, as well as *ex situ* SEM and X-ray diffraction (XRD) analyses of the LiFePO₄ cathode.

The EIS investigation on the Li/LFP cells has been carried out by employing a three-electrode configuration that can reveal the actual contribution of cathode and anode interphases on the overall cell resistance (see Figures 4 and S3a-d in the Supporting Information). Thus, impedance spectra of the LFP and Li electrodes have been recorded at the open circuit voltage (OCV) and after 1, 10, 100 and 200 cycles (see the related Nyquist plots of main panels and insets of Figure 4, respectively) and analyzed through a nonlinear least squares (NLLS) fit procedure^[77] using an equivalent circuit that takes into account a high-frequency response ascribed to the electrolyte resistance (R_e), a middle-high frequency response attributed to n interphase pseudocapacitances (Q_i) and resistances (R_i) reflecting the passivation layer, the charge transfer and the double layer ($i = 1, 2, \dots, n$), and a low-frequency pseudocapacitance attributed to the Warburg-type Li⁺ diffusion.^[78] The analysis suggests a remarkable increase of the overall LFP/electrolyte interphase resistance (ΣR_i) at the 200th cycle for the cells using solutions A, B, and C (see Figure 4a-c and Figure S3a in the Supporting Information). On the other hand, the lithium/electrolyte interphase resistance (Figure 4a-c insets and Figure S3c in the Supporting Information) fluctuates below 120 Ω suggesting that the evolution of the SEI over the anode during 200 cycles does not significantly hinder the Li⁺ diffusion.^[79] As for solutions D, E, and F, EIS indicates rather stable interphases over both LFP and Li, with ΣR_i values permanently below 150 Ω during 200 cycles. Notably, the results of panels c and d of Figure 1 indicate an excellent stability of the lithium/electrolyte interphase both under static and dynamic conditions for all the investigated formulations, which is in full agreement with the results of Figure 4, although particular glyme-based compositions may be poorly compatible with lithium metal.^[80] Therefore, the significant increase in cathode/electrolyte interphase resistance for the DEGDME-containing cells might partially account for the capacity fading observed in Figure 2. However, the change of slope in the voltage curves of Figure 2a, c, and e suggests an additional phenomenon besides the interphase

resistance increase, possibly affecting the kinetics of the Li^+ insertion process. XRD and SEM measurements on the cycled LFP electrodes shed light on this point.

Figure 4

We have collected SEM images and XRD patterns of the LFP electrodes before and after 200 cycles in the lithium cells. The related results are shown in Figures S4 of the Supporting Information and in Figure 5. SEM suggests the deposition of a passivation layer over the spherical agglomerates of primary LFP particles (compare Figure S4a with Figure 5a-f) along with a minor rearrangement occurring in the spherulites possibly due to structural modifications. Such phenomena are particularly relevant for electrolytes B and C, and partially in agreement with the EIS response of the positive electrode (Figures 4 and S3 in the Supporting Information). XRD reveals an increase in the full width at half maximum (FWHM) for the olivine during cycling (compare Figure S4b in the Supporting Information with Figure 5g and h), which might be associated with the change in voltage profile slope for the DEGDME-containing cells (see Figure 2a, c, and e). Indeed, the significant decrease in the average crystallite size may affect the voltage profile by changing either the local biphasic voltage or the insertion mechanism from a two-phase transformation to a single-phase, diffusion-limited process.^[75,76]

Figure 5

Hence, we have subsequently carried out a detailed study of the electrolyte E (LiTFSI-LiNO₃-TREGDME) aiming at assessing the Li/LFP cell behavior upon long-term cycling by coupling galvanostatic charge/discharge and impedance measurements. Figure 6a reports the cycling response of the cell at 1C, 2C, and 5C rates (1C = 170 mA g⁻¹) as trend of discharge capacity and coulombic efficiency. After the initial electrochemical activation of the LFP cathode,^[72] the battery delivers capacities of about 147 mAh g⁻¹ at 1C and 138 mA h g⁻¹ at 2C and 5C rates, slightly decreasing to 144, 137 and 131 mA h g⁻¹ at the 200th cycle. Coulombic efficiency values approaching 100% further indicate reversible reaction with low electrolyte decomposition and suggest stable electrode/electrolyte interphases. This trend appears remarkable, in particular considering the

relatively high current rates used for cycling (that is, 1C, 2C and 5C), however the discharge capacity decreases to values within the range from 103 and 106 mA h g⁻¹ at the 500th cycle. Hence, the partial fading likely suggests possible effects of the cycling conditions on the phenomena occurring in the cell by the increase of the employed current.^[81] The stability of electrode/electrolyte interphases at both the anode and the cathode sides may play a crucial role for the cell response upon prolonged charge/discharge cycles.^[82] Herein, EIS measurements carried out during cycling shed light on the cell resistance trend throughout the tests. Thus, panels b, c, and d of Figure 6 display the evolution of the related Nyquist plots at 1C, 2C and 5C rates, respectively. Each spectrum consists of overlapped high-to-middle frequency semicircles and a middle-to-low frequency response which substantially modifies from the OCV to the following cycles. These impedance features are likely attributed to the passivation films and charge transfer processes at the electrode/electrolyte interphases as well as to Li⁺ diffusion phenomena and geometrical capacitance.^[83] Accordingly the spectra have been analyzed by a NLLS method using an equivalent circuit formed by an arrangement of resistance and pseudo-capacitance elements as reported in Table 1, where R_e is the electrolyte resistance at high frequency, the (R_iQ_i) (i = 1, 2, ... ,n) sub-circuits account for the contribution of the electrode/electrolyte interphase resistances (R_i) and capacitances (Q_{1,2, ... ,n}) at high-to-middle frequency, (R_dQ_d) is a diffusion element at low frequency, and Q_g is a geometrical capacitance clearly observed at in the Nyquist plots the OCV as a vertical line at low frequency.^[84] The χ^2 values mostly below 10⁻⁴ confirm the reliability of the analysis (see Table 1). As mentioned, after the 1st cycle EIS reveals a remarkable change in the low-frequency region of the spectra from a quasi-capacitive to a diffusion-type response, along with a significant decrease of the interphase resistance (ΣR_i , see Figure 4e). This drop may partially account for the electrochemical activation (increase of capacity) observed during the very first cycles of the galvanostatic measurement (see Figure 6a). However, the NLLS analysis suggests a significant hindering to the Li⁺ diffusion over the following cycles in spite of relatively stable high-to-middle frequency resistance values. Although the slow Li⁺ diffusion might partially reflect the capacity fading trend at the various rates, the favorable characteristics of the interphases at

the anode and the cathode sides (compare panel a and e of Figure 6 and Table 1) ensure a promising cell behavior over 500 cycles for a possible application of the glyme-based electrolyte. Relevantly, the absence of any dendrite evolution, the relatively high delivered capacity (i.e., over 100 mAh g⁻¹) at elevated current rates (up to 5C), and a capacity retention exceeding 70% upon 500 charge/discharge cycles are actually remarkable characteristics which may contribute to the development of a rechargeable lithium-metal cell operating at room temperature.

Figure 6

Conclusion

Diglyme and triglyme-based solutions using LiFSI, LiTFSI and LiBETI, and enhanced by the LiNO₃ additive, were investigated for a possible application in lithium-metal batteries employing the LiFePO₄ cathode. A detailed electrochemical study revealed optimal characteristics in terms of ionic transport and stability against the lithium-metal anode. Thus, the solutions exhibited room-temperature ionic conductivity within 10⁻³ and 10⁻² S cm⁻¹ and lithium transference number higher than 0.6. Cyclic voltammetry suggested that the LiNO₃ reduction between 1.7 and 1.4 V vs. Li⁺/Li may lead to a stable lithium/electrolyte interphase with low resistance (ranging from 20 to 30 Ω cm⁻²) and suitable lithium plating/stripping for prolonged cycling. An oxidative stability over 4.3 V vs. Li⁺/Li ensured promising electrochemical performances in Li/LiFePO₄ cells with reversible capacity of the order of 150 mAh g⁻¹ at a C/3 rate (1C = 170 mA g⁻¹) and coulombic efficiency above 99% upon 200 cycles. However, the diglyme-based cells showed a capacity fading to about 140 (for LiFSI) and 130 mAh g⁻¹ (LiTFSI and LiBETI), while the triglyme-based ones exhibit an outstanding performance without any evidence of degradation after 200 cycles and coulombic efficiency values above 99.6%. Notably, a change in voltage profile slope occurring in the cells using the diglyme may be directly associated with the observed capacity fading and with a concurrent increase of the cathode/electrolyte interphase resistance. Indeed, EIS and SEM measurement suggested the precipitation of a passivation layer on the positive electrode, while the SEI over the lithium-metal

anode appeared to be relatively stable and suitably permeable to the Li^+ ions. Moreover, the cycling with diglyme has led to a decrease in the average crystallite size of the olivine phase, as suggested by *ex situ* XRD, with minor rearrangements of the primary particles forming the LFP spherulites. Such microstructural reorganizations were supposed to affect the Li^+ insertion kinetics and the redox potential, thereby possibly altering the voltage profile of the cell.^[75,76]

Our results confirmed previous observations^[31,32] on the beneficial effect of LiNO_3 on both the positive and negative interphases, thus suggesting that the electrochemical stability of a particular glyme-based electrolyte formulation against the cathode is not exclusively related to the electrochemical stability window. Indeed, LiNO_3 ensured the formation of a stable interphase at the anode for all the electrolyte formulations, although the glyme length affected the interphase behavior at the cathode, while the anion composition within the investigated sulfonimide family slightly altered the cell response. Among the various electrolyte formulations, the one using triglyme, LiTFSI and LiNO_3 was selected as the most promising combination. Therefore, EIS measurements throughout galvanostic charge/discharge tests for 500 cycles revealed a capacity of about 150 mAh g^{-1} at 1C, and 140 mAh g^{-1} at 2C and 5C rates, which decreased to values within 103 and 106 mAh g^{-1} , as well as relatively stable SEI and charge transfer resistance at medium-high frequency ascribed to coulombic efficiency values approaching 100%. Hence, our results suggested the possible applicability of glyme-based, LiNO_3 -containing solutions in high-energy lithium-metal batteries.

Experimental

Electrolyte Preparation

Diethylene glycol dimethyl ether ($(\text{CH}_3\text{OCH}_2\text{CH}_2)_2\text{O}$, DEGDME, Sigma-Aldrich) and triethylene glycol dimethyl ether ($(\text{CH}_3(\text{OCH}_2\text{CH}_2)_3\text{OCH}_3$, TREGDME, Sigma-Aldrich) were dried over 5 Å molecular sieves before use. The final water content was below 10 ppm according to the Karl Fischer titration (899 KF Coulometer, Metrohm). Lithium bis(fluorosulfonyl)imide (LiFSI, Sigma-Aldrich), lithium bis(trifluoromethanesulfonyl)imide (LiTFSI, Sigma-Aldrich), lithium

bis(pentafluoroethanesulfonyl)imide (LiBETI, Sigma-Aldrich), and lithium nitrate (LiNO_3 , Sigma-Aldrich) were dried under vacuum at $110\text{ }^\circ\text{C}$ for 24 h prior to use. Six electrolyte solutions were obtained by dissolving LiFSI, LiTFSI, LiBETI salts either in DEGDME or TREGDME solvents, respectively, by using a concentration of 1 mol kg^{-1} with respect to the solvent. LiNO_3 was added to above electrolyte solutions with a concentration of 0.4 mol of salt in 1 kg of solvent. Table 2 reports in detail the electrolyte compositions and sample acronyms (that is, A-F, respectively). The electrolyte preparation was performed in an Ar-filled glovebox (O_2 and H_2O content below 1 ppm).

Table 2

Electrode and Cell Preparation

LiFePO_4 was studied previously.^[85] The cathode slurry was made by blending LFP, super P carbon (Timcal), and polyvinylidene fluoride (PVDF 6020, Solvay) in N-methyl pyrrolidone (NMP, Sigma-Aldrich) solvent with a composition of 80:10:10 by weight. The slurry was homogeneously cast onto an aluminum foil through a doctor blade, then dried at $70\text{ }^\circ\text{C}$ for about 3 h under the air on a hot plate. Subsequently, the coated foil was cut into circular electrodes with a diameter of 14 mm and dried at $110\text{ }^\circ\text{C}$ under vacuum for about 3 h before use. The final mass loading of LFP ranged from about 3.8 mg cm^{-2} to 4.4 mg cm^{-2} . Carbon-based electrodes containing 80% of super P and 20% of PVDF were also prepared according to the above described procedure, by casting on either aluminum (carbon-coated aluminum) or copper (carbon-coated copper) foils through a doctor blade. The C-coated aluminum and copper foils were cut into disks with a diameter of 10 mm and then dried at $110\text{ }^\circ\text{C}$ under vacuum for about 3 h before use.

Two- and three-electrode T-type cells were assembled by using glass fiber separators (Whatman[®], GF/A) soaked by the electrolyte solution, lithium-metal disks, and carbon-based electrodes deposited on aluminum/copper current collector with a diameter of 10 mm (0.785 cm^2). Coin cells (CR2032, MTI Corporation) were made by using lithium-metal disks, LFP electrodes with a diameter of 14 mm (1.54 cm^2), and glass fiber separators (Whatman[®], GF/A) with diameter of 16

mm soaked by the electrolyte solution. All the cells were assembled in an Ar-filled glovebox (O₂ and H₂O content below 1 ppm).

Electrolyte Characterization

The ionic conductivity of the electrolyte solutions (A-F) was measured within the temperature range from 0 to 80 °C by EIS through a Princeton Applied Research Potentiostat/Galvanostat (PAR, VersaSTAT MC), employing an alternate voltage signal with amplitude of 10 mV within the 500 kHz – 10 Hz frequency range. EIS was performed on symmetric stainless steel/electrolyte/stainless steel CR2032 coin-cells, using a Teflon separator to fix the cell constant ($1.27 \times 10^{-2} \text{ cm}^{-1}$). Each conductivity value was measured every 10 °C during a cooling scan, after at least 6 h of cell conditioning at a constant temperature.

The lithium transference number (t^+) was evaluated by the electrochemical method proposed by Evans *et al.*^[47] combining chronoamperometry and EIS measurements. Accordingly, t^+ was calculated by following the equation 1^[47]:

$$t^+ = \frac{I_{SS} (\Delta V - I_0 R_0)}{I_0 (\Delta V - I_{SS} R_{SS})} \quad (1)$$

where I_0 and I_{SS} refer to the initial and steady-state current values of the chronoamperometry measurements, respectively, R_0 and R_{SS} represent the charge-transfer resistance between lithium and electrolyte before and after polarization, respectively, and ΔV is the applied voltage. R_0 and R_{SS} were calculated by a NLLS analysis of the impedance spectra,^[77] in which the Warburg region at low frequency has not been considered.^[86–88] Chi-square parameters below 10^{-4} further confirm the reliability of the fitting method. Chronoamperometry was carried out on two-electrode, T-type symmetrical Li/Li cells, by applying a 30 mV (ΔV) direct current (DC) pulse for 90 min, while EIS measurement was performed by using an alternating current (AC) signal with an amplitude of 10 mV within the 500 kHz – 100 mHz frequency range. Chronoamperometry was performed by adjusting the time intervals for data collection in order to get accurate I_0 and I_{SS} values: intervals of 0.05 and 10 s point^{-1} were used within the time ranges from 0 (initial state) to 300 s and from 300 s to 90 min

(steady state), respectively. The cells for t^+ employed 10 glass fiber separators in order to increase the electrolyte resistance and allow the accuracy of the method.^[45] The experiments for t^+ determination were performed through a Princeton Applied Research Potentiostat/Galvanostat (PAR, VersaSTAT MC). The errors on t^+ was estimated to be within 0.06 and 0.07 (*i.e.*, 10%) taking into account errors on current and resistance lower than 1% and 5%.

The electrochemical stability window was investigated by LSV and CV at a scan rate of 0.1 mV s⁻¹ in high-potential and low-potential range, respectively. The LSV measurement was conducted from the OCV (about 3 V) to about 5 V *vs.* Li⁺/Li by using lithium-metal disks as the counter and reference electrodes and carbon-coated aluminum as the working electrode (three-electrode T-type configuration), while CV test was performed within 0.01 – 2 V *vs.* Li⁺/Li potential range by using the same cells configuration with carbon-coated copper as working electrode. The LSV and CV measurements were carried out through a Princeton Applied Research Potentiostat/Galvanostat (PAR, VersaSTAT MC).

EIS measurements on symmetrical Li/Li coin-cells were performed upon aging for 31 days to evaluate the stability of lithium/electrolyte interphase by applying an alternate voltage signal with amplitude of 10 mV within the 500 kHz – 100 mHz frequency range through SP-200 system a SP-200 Potentiostat (Bio-Logic Instrument). The EIS measurements have been repeated twice in order to confirm the trends of interphase resistance. The lithium stripping/deposition process was investigated by using symmetrical Li/Li coin-cells through a HJ1001SM8A system (Hokuto Denko Co.). A constant current of 0.1 mA cm⁻² was applied to the cell by alternating charge and discharge steps of 60 min. All the measurements except the EIS to estimate the ionic conductivity were performed at 25 °C.

Tests in Lithium-Metal Cell

The electrolyte solutions (A-F) were studied in Li/LFP coin-cells by galvanostatic charge/discharge cycling at a C/3 rate (1C = 170 mA g⁻¹) upon 200 cycles using a voltage range of

2.8 – 3.9 V. These experiments were carried out through a HJ1001SM8A system (Hokuto Denko Co.). EIS measurements were done on 3-electrode T-type Li/LFP cells using a lithium probe at the OCV as well as after 1st, 10th, 100th and 200th cycles. These cells were cycled at a C/3 rate (1C = 170 mA g⁻¹) upon 200 cycles using a voltage range of 2 – 4 V by a MACCOR Series 4000 battery test system in a two-electrode configuration. EIS was carried out by applying an alternate voltage signal with amplitude of 10 mV within 500 kHz – 20 mHz frequency range through a Princeton Applied Research Potentiostat/Galvanostat (PAR, VersaSTAT MC). All the EIS spectra were analyzed and processed by the Boukamp software according to a NLLS method.^[77]

Li/LFP coin-cells using the E solution (see Table 2 for acronym) were also tested at 1C, 2C, and 5C rates upon 500 cycles within the 2.8 – 3.9 V, 2.8 – 4.0 V, 2.0 – 4.1 V voltage ranges, respectively, through a MACCOR Series 4000 battery test system. EIS measurements were carried out during the 500-cycle tests at the OCV, 1st, 200th, and 500th cycles, respectively. The EIS measurements were carried out by applying an alternate voltage signal with amplitude of 10 mV within the 500 kHz – 100 mHz frequency range through a Princeton Applied Research Potentiostat/Galvanostat (PAR, VersaSTAT MC). All the cycling test and the related EIS measurements were performed at 25 °C. All the EIS spectra were analyzed by the Boukamp software according to a NLLS method.^[77]

Ex Situ Analysis of the Cycled LiFePO₄ Electrodes

Structure and morphology of LFP electrodes before and after 200 cycles in the various lithium cells using the glyme solutions were investigated by XRD and SEM. After cell disassembly, the cathodes were rinsed with dimethyl carbonate (DMC) to remove possible residuals and dried under vacuum for about 3 min. XRD patterns were collected through a Bruker D8-Advance using a Cu K α source, by performing a scan in the 2 θ range from 10 to 80° with a step size of 0.02° and a rate of 10 s step⁻¹. SEM images were taken by a Zeiss EVO 40 microscope equipped with a LaB₆ and tungsten thermionic gun.

Acknowledgments

This work was founded by the grant “Fondo di Ateneo per la Ricerca Locale (FAR) 2018”, University of Ferrara, and by the Institute of Global Innovation Research (GIR) in Tokyo University of Agriculture and Technology, and performed within the collaboration project “Accordo di Collaborazione Quadro 2015” between University of Ferrara (Department of Chemical and Pharmaceutical Sciences) and Sapienza University of Rome (Department of Chemistry).

References

- [1] M. Li, J. Lu, Z. Chen, K. Amine, *Adv. Mater.* **2018**, *30*, 1800561.
- [2] D. Di Lecce, R. Verrelli, J. Hassoun, *Green Chem.* **2017**, *19*, 3442.
- [3] D. Di Lecce, C. Fasciani, B. Scrosati, J. Hassoun, *ACS Appl. Mater. Interfaces* **2015**, *7*, 21198.
- [4] V. Aravindan, Y.-S. Lee, S. Madhavi, *Adv. Energy Mater.* **2015**, *5*, 1402225.
- [5] X. Shen, Y. Li, T. Qian, J. Liu, J. Zhou, C. Yan, J. B. Goodenough, *Nat. Commun.* **2019**, *10*, 900.
- [6] W. Xu, J. Wang, F. Ding, X. Chen, E. Nasybulin, Y. Zhang, J.-G. Zhang, *Energy Environ. Sci.* **2014**, *7*, 513.
- [7] C. Sun, J. Liu, Y. Gong, D. P. Wilkinson, J. Zhang, *Nano Energy* **2017**, *33*, 363.
- [8] D. Lin, Y. Liu, Y. Cui, *Nat. Nanotechnol.* **2017**, *12*, 194.
- [9] J. Qian, W. A. Henderson, W. Xu, P. Bhattacharya, M. Engelhard, O. Borodin, J.-G. Zhang, *Nat. Commun.* **2015**, *6*, 6362.
- [10] L. Zhang, Z. Chen, N. Dongfang, M. Li, C. Diao, Q. Wu, X. Chi, P. Jiang, Z. Zhao, L. Dong, R. Che, K. P. Loh, H. Lu, **2018**, *1802431*, 1.

- [11] X. Gao, X. Yang, M. Li, Q. Sun, J. Liang, J. Luo, J. Wang, W. Li, J. Liang, Y. Liu, S. Wang, Y. Hu, Q. Xiao, R. Li, T. K. Sham, X. Sun, *Adv. Funct. Mater.* **2019**, *29*, 1806724.
- [12] J. O. Park, M. Kim, J. H. Kim, K. H. Choi, H. C. Lee, W. Choi, S. B. Ma, D. Im, *J. Power Sources* **2019**, *419*, 112.
- [13] Z. Zhang, C. Yang, S. Wu, A. Wang, L. Zhao, D. Zhai, B. Ren, K. Cao, Z. Zhou, *Adv. Energy Mater.* **2018**, *1802805*, 1.
- [14] W. Li, H. Yao, K. Yan, G. Zheng, Z. Liang, Y.-M. Chiang, Y. Cui, *Nat. Commun.* **2015**, *6*, 7436.
- [15] C. Yan, Y. X. Yao, X. Chen, X. B. Cheng, X. Q. Zhang, J. Q. Huang, Q. Zhang, *Angew. Chemie - Int. Ed.* **2018**, *57*, 14055.
- [16] X. Fan, L. Chen, O. Borodin, X. Ji, J. Chen, S. Hou, T. Deng, J. Zheng, C. Yang, S.-C. Liou, K. Amine, K. Xu, C. Wang, *Nat. Nanotechnol.* **2018**, *13*, 715.
- [17] J. Zheng, M. Tang, Y. Y. Hu, *Angew. Chemie - Int. Ed.* **2016**, *55*, 12538.
- [18] S. Choi, M. Eom, S. Son, L. Choi, D. Shin, C. Park, *J. Power Sources* **2016**, *331*, 26.
- [19] P. Knauth, *Solid State Ionics* **2009**, *180*, 911.
- [20] J. Hassoun, R. Verrelli, P. Reale, S. Panero, G. Mariotto, S. Greenbaum, B. Scrosati, *J. Power Sources* **2013**, *229*, 117.
- [21] D. Di Lecce, V. Sharova, S. Jeong, A. Moretti, S. Passerini, *Solid State Ionics* **2018**, *316*, 66.
- [22] J.-D. Xie, W.-J. Liu, C. Li, J. Patra, Y. A. Gandomi, Q.-F. Dong, J.-K. Chang, *Electrochim. Acta* **2019**, *319*, 625.
- [23] D. Shanmukaraj, S. Lois, S. Fantini, F. Malbosc, M. Armand, *Chem. Mater.* **2018**, *30*, 246.
- [24] W. A. Henderson, *Macromolecules* **2007**, *40*, 4963.

- [25] L. Carbone, M. Gobet, J. Peng, M. Devany, B. Scrosati, S. Greenbaum, J. Hassoun, *ACS Appl. Mater. Interfaces* **2015**, *7*, 13859.
- [26] A. Benítez, D. Di Lecce, Á. Caballero, J. Morales, E. Rodríguez-Castellón, J. Hassoun, *J. Power Sources* **2018**, *397*, 102.
- [27] D. Morales, R. E. Ruther, J. Nanda, S. Greenbaum, *Electrochim. Acta* **2019**, *304*, 239.
- [28] S. Tobishima, H. Morimoto, M. Aoki, Y. Saito, T. Inose, T. Fukumoto, T. Kuryu, *Electrochim. Acta* **2004**, *49*, 979.
- [29] B. Qin, S. Jeong, H. Zhang, U. Ulissi, D. Vieira Carvalho, A. Varzi, S. Passerini, *ChemSusChem* **2019**, *12*, 208.
- [30] L. Carbone, P. T. Moro, M. Gobet, S. Munoz, M. Devany, S. G. Greenbaum, J. Hassoun, *ACS Appl. Mater. Interfaces* **2018**, *10*, 16367.
- [31] L. Carbone, D. Di Lecce, M. Gobet, S. Munoz, M. Devany, S. Greenbaum, J. Hassoun, *ACS Appl. Mater. Interfaces* **2017**, *9*, 17085.
- [32] L. Carbone, M. Gobet, J. Peng, M. Devany, B. Scrosati, S. Greenbaum, J. Hassoun, *J. Power Sources* **2015**, *299*, 460.
- [33] A. Unemoto, S. Ueda, E. Seki, M. Oda, J. Kawaji, T. Okumura, Y. Gambe, I. Hinma, *Electrochemistry* **2019**, *87*, 100.
- [34] T. Yang, W. Fan, C. Wang, Q. Lei, Z. Ma, L. Yu, X. Zuo, J. Nan, *ACS Appl. Mater. Interfaces* **2018**, *10*, 31735.
- [35] J. Li, J. Wang, X. He, L. Zhang, A. Senyshyn, B. Yan, M. Muehlbauer, X. Cao, B. Vortmann-Westhoven, V. Kraft, H. Liu, C. Luerenbaum, G. Schumacher, E. Paillard, M. Winter, J. Li, *J. Power Sources* **2019**, *416*, 184.
- [36] J. Lee, Y.-J. Kim, H. S. Jin, H. Noh, H. Kwack, H. Chu, F. Ye, H. Lee, H.-T. Kim, *ACS*

Omega **2019**, *4*, 3220.

- [37] S. Xiong, K. Xie, Y. Diao, X. Hong, *Electrochim. Acta* **2012**, *83*, 78.
- [38] A. Ramanujapuram, G. Yushin, *Adv. Energy Mater.* **2018**, *8*, 1.
- [39] A. Rosenman, R. Elazari, G. Salitra, E. Markevich, D. Aurbach, A. Garsuch, *J. Electrochem. Soc.* **2015**, *162*, A470.
- [40] D. Di Lecce, V. Marangon, A. Benítez, Á. Caballero, J. Morales, E. Rodríguez-Castellón, J. Hassoun, *J. Power Sources* **2019**, *412*, 575.
- [41] F. Qiu, X. Li, H. Deng, D. Wang, X. Mu, P. He, H. Zhou, *Adv. Energy Mater.* **2019**, *9*, 1803372.
- [42] B. D. Adams, E. V. Carino, J. G. Connell, K. S. Han, R. Cao, J. Chen, J. Zheng, Q. Li, K. T. Mueller, W. A. Henderson, J.-G. Zhang, *Nano Energy* **2017**, *40*, 607.
- [43] L. Carbone, S. G. S. G. Greenbaum, J. Hassoun, *Sustain. Energy Fuels* **2017**, *1*, 228.
- [44] D. Di Lecce, L. Carbone, V. Gancitano, J. Hassoun, *J. Power Sources* **2016**, *334*, 146.
- [45] S. Wei, Z. Li, K. Kimura, S. Inoue, L. Pandini, D. Di Lecce, Y. Tominaga, J. Hassoun, *Electrochim. Acta* **2019**, *306*, 85.
- [46] K. Xu, *Chem. Rev.* **2014**, *114*, 11503.
- [47] J. Evans, C. a. Vincent, P. G. Bruce, *Polymer.* **1987**, *28*, 2324.
- [48] H. Hirayama, N. Tachikawa, K. Yoshii, M. Watanabe, Y. Katayama, *Electrochemistry* **2015**, *83*, 824.
- [49] K. Yoshida, M. Tsuchiya, N. Tachikawa, K. Dokko, M. Watanabe, *J. Phys. Chem. C* **2011**, *115*, 18384.
- [50] S. Seki, K. Takei, H. Miyashiro, M. Watanabe, *J. Electrochem. Soc.* **2011**, *158*, A769.

- [51] J. Popovic, D. Höfler, J. P. Melchior, A. Münchinger, B. List, J. Maier, *J. Phys. Chem. Lett.* **2018**, *9*, 5116.
- [52] C. Pfaffhuber, F. Hoffmann, M. Froba, J. Popovic, J. Maiera, *J. Mater. Chem. A* **2013**, *1*, 12560.
- [53] J. Peng, L. Carbone, M. Gobet, J. Hassoun, M. Devany, S. Greenbaum, *Electrochim. Acta* **2016**, *213*, 606.
- [54] Y. Ma, *J. Electrochem. Soc.* **1995**, *142*, 1859.
- [55] S. Zugmann, M. Fleischmann, M. Amereller, R. M. Gschwind, H. D. Wiemhöfer, H. J. Gores, *Electrochim. Acta* **2011**, *56*, 3926.
- [56] D. Di Lecce, L. Minnetti, D. Polidoro, V. Marangon, J. Hassoun, *Ionics*. **2019**, *25*, 3129.
- [57] J. Popovic, in *Encycl. Inorg. Bioinorg. Chem.*, Wiley, **2019**, pp. 1–11.
- [58] J. Popovic, G. Hasegawa, I. Moudrakovski, J. Maier, *J. Mater. Chem. A* **2016**, *4*, 7135.
- [59] A. K. Padhi, *J. Electrochem. Soc.* **1997**, *144*, 1188.
- [60] D. Di Lecce, J. Hassoun, *J. Phys. Chem. C* **2015**, *119*, 20855.
- [61] E. Krämer, T. Schedlbauer, B. Hoffmann, L. Terborg, S. Nowak, H. J. Gores, S. Passerini, M. Winter, *J. Electrochem. Soc.* **2013**, *160*, A356.
- [62] K. Yoshida, M. Nakamura, Y. Kazue, N. Tachikawa, S. Tsuzuki, S. Seki, K. Dokko, M. Watanabe, *J. Am. Chem. Soc.* **2011**, *133*, 13121.
- [63] C. Zhang, A. Yamazaki, J. Murai, J. W. Park, T. Mandai, K. Ueno, K. Dokko, M. Watanabe, *J. Phys. Chem. C* **2014**, *118*, 17362.
- [64] K. Xu, *Chem. Rev.* **2004**, *104*, 4303.
- [65] M. Morita, T. Shibata, N. Yoshimoto, M. Ishikawa, *Electrochim. Acta* **2002**, *47*, 2787.

- [66] K. Park, S. Yu, C. Lee, H. Lee, *J. Power Sources* **2015**, 296, 197.
- [67] L. Carbone, T. Coneglian, M. Gobet, S. Munoz, M. Devany, S. Greenbaum, J. Hassoun, *J. Power Sources* **2018**, 377, 26.
- [68] D.-J. Yoo, K. J. Kim, J. W. Choi, *Adv. Energy Mater.* **2018**, 8, 1702744.
- [69] M. Gauthier, T. J. Carney, A. Grimaud, L. Giordano, N. Pour, H.-H. Chang, D. P. Fenning, S. F. Lux, O. Paschos, C. Bauer, F. Maglia, S. Lupart, P. Lamp, Y. Shao-Horn, *J. Phys. Chem. Lett.* **2015**, 6, 4653.
- [70] S. Xiong, Y. Diao, X. Hong, Y. Chen, K. Xie, *J. Electroanal. Chem.* **2014**, 719, 122.
- [71] K. Zhang, G. H. Lee, M. Park, W. Li, Y. M. Kang, *Adv. Energy Mater.* **2016**, 6, 1.
- [72] D. Di Lecce, R. Brescia, A. Scarpellini, M. Prato, J. Hassoun, *ChemSusChem* **2016**, 9, 223.
- [73] Y. Zhang, C.-Y. Wang, X. Tang, *J. Power Sources* **2011**, 196, 1513.
- [74] K. Zaghbi, A. Guerfi, P. Hovington, A. Vijh, M. Trudeau, A. Mauger, J. B. Goodenough, C. M. Julien, *J. Power Sources* **2013**, 232, 357.
- [75] N. Meethong, Y.-H. Kao, W. C. Carter, Y.-M. Chiang, *Chem. Mater.* **2010**, 22, 1088.
- [76] A. Van der Ven, M. Wagemaker, *Electrochem. commun.* **2009**, 11, 881.
- [77] B. A. Boukamp, *Solid State Ionics* **1986**, 20, 31.
- [78] D. Di Lecce, V. Gancitano, J. Hassoun, *ACS Sustain. Chem. Eng.* **2020**, 8, 278.
- [79] G. A. Elia, U. Ulissi, S. Jeong, S. Passerini, J. Hassoun, *Energy Environ. Sci.* **2016**, 9, 3210.
- [80] D. Aurbach, G. Eran, E. Granot, *Electrochim. Acta* **1997**, 42, 697.
- [81] S. S. Zhang, *J. Power Sources* **2006**, 161, 1385.
- [82] G. A. Elia, U. Ulissi, F. Mueller, J. Reiter, N. Tsiouvaras, Y.-K. Sun, B. Scrosati, S.

- Passerini, J. Hassoun, *Chem. - A Eur. J.* **2016**, *22*, 6808.
- [83] D. Di Lecce, R. Verrelli, J. Hassoun, *Electrochim. Acta* **2016**, *220*, 384.
- [84] D. Di Lecce, D. Campanella, J. Hassoun, *J. Phys. Chem. C* **2018**, *122*, 23925.
- [85] S. Brutti, J. Hassoun, B. Scrosati, C.-Y. Y. Lin, H. Wu, H.-W. W. Hsieh, *J. Power Sources* **2012**, *217*, 72.
- [86] T. Q. Nguyen, C. Breitkopf, *J. Electrochem. Soc.* **2018**, *165*, E826.
- [87] P. Ravn Sørensen, T. Jacobsen, *Electrochim. Acta* **1982**, *27*, 1671.
- [88] F. Wohde, M. Balabajew, B. Roling, *J. Electrochem. Soc.* **2016**, *163*, A714.

Table captions

Table 1. Results of NLLS analysis^[77] of EIS data collected throughout galvanostatic cycling tests at 1C, 2C and 5C rates (1C = 170 mA g⁻¹) of electrolyte E (LiTFSI-LiNO₃-TREGDME) in a Li/LiFePO₄ cell. In detail: C rate, cycle life, equivalent circuit, χ^2 , and sum of electrode/electrolyte interphase resistances ($\sum R_i$, Ω , $i = 1, 2, \dots, n$) at high-medium frequency. See the related cycling trend and Nyquist plots in Figure 4 and the electrolytes' acronym in Table 2.

Table 2. Overview of all electrolyte solutions and corresponding sample acronyms (A-F) used in this work.

Figure captions

Figure 1. Electrochemical properties of the electrolyte solutions studied in this work. **(a)** Temperature dependence of ionic conductivity as obtained by EIS. Inset: lithium transference number (t^+) at 25 °C as determined by the electrochemical method proposed by Evans *et al.* [47] See Figure S1 and Table S1 in the Supporting Information for the chronoamperometry profiles and Nyquist plots related to the t^+ evaluation. **(b)** Electrochemical stability window assessed by linear sweep voltammetry (LSV, high-potential region) and cyclic voltammetry (CV, low-potential region) at 0.1 mV s⁻¹ of three-electrode lithium cells using carbon-coated Al and Cu working electrodes, respectively, with magnifications in inset. **(c)** Time evolution of the lithium/electrolyte interphase resistance as determined by EIS measurements on symmetrical Li/Li cells. See Figure S2 and Table S2 in the Supporting Information for the related Nyquist plots. **(d)** Voltage profiles of lithium deposition/stripping tests at a constant current of 0.1 mA cm⁻² on Li/Li symmetrical cells (step time: 1h) with magnification in inset. See the experimental section for details of the procedures.

Figure 2. Cycling performances over 200 cycles of Li/LiFePO₄ cells using electrolytes **(a-b)** A, **(c-d)** B and **(e-f)** C at a C/3 rate (1C = 170 mA g⁻¹) in terms of **(a, c, e)** voltage profiles of the 1st, 5th, 10th, 25th, 50th, 100th, 150th, 200th cycles and **(b, d, f)** discharge capacity trend (left y-axis) with coulombic efficiency (right- y-axis). See Table 2 for electrolytes' acronyms.

Figure 3. Cycling performances over 200 cycles of Li/LiFePO₄ cells using electrolytes **(a-b)** D, **(c-d)** E and **(e-f)** F solutions at a C/3 rate (1C = 170 mA g⁻¹) in terms of **(a, c, e)** voltage profiles of the 1st, 5th, 10th, 25th, 50th, 100th, 150th, 200th cycles and **(b, d, f)** discharge capacity trend (left y-axis) with coulombic efficiency (right- y-axis). See Table 2 for electrolytes' acronyms.

Figure 4. Nyquist plots of EIS measurements of the (main panels) positive LFP and (inset) negative Li electrodes performed in three-electrode, T-type cells using lithium metal as the reference electrode and solutions **(a)** A, **(b)** B, **(c)** C, **(d)** D, **(e)** E, and **(f)** F as the electrolyte; spectra recorded at the OCV and after the 1st, 10th, 100th and 200th cycles at a 2C rate (1C = 170 mA g⁻¹, see Figure 2 and 3 for

further details), by employing a signal amplitude of 10 mV within the frequency range from 500 kHz to 20 mHz. Temperature: 25 °C. See Table 2 for electrolytes' acronyms.

Figure 5. (a-f) *Ex situ* SEM images of the LFP electrodes recovered from the lithium cells analyzed in Figure 4, disassembled after 200 cycles at a 2C rate ($1C = 170 \text{ mA g}^{-1}$, see the SEM image of pristine LFP in Figure S4 of the Supporting information); cells using electrolytes **(a)** A, **(b)** B, **(c)** C, **(d)** D, **(e)** E, and **(f)** F. **(g-h)** XRD patterns of the same LFP electrodes materials (using electrolyte **(g)** A, B and C, and electrolytes **(h)** D, E and F) and of a pristine LFP electrode. Cathodes rinsed with dimethyl carbonate (DMC) and dried under vacuum for about 3 min after cell disassembly.

Figure 6. (a) Galvanostatic cycling trend in terms of discharge capacity (left y-axis) with coulombic efficiency (right- y-axis) over 500 cycles of a Li/LiFePO₄ cell using electrolyte E (LiTFSI-LiNO₃-TREGDME) at 1C, 2C and 5 C rates ($1C = 170 \text{ mA g}^{-1}$). **(b, c, d)** Nyquist plots of EIS measurements performed on the Li/LiFePO₄ cell using electrolyte E during the cycling tests at **(b)** 1C, **(c)** 2C and **(d)** 5C rates. Impedance spectra were carried out at open-circuit voltage (OCV), after the 1st, 200th and 500th cycle. **(e)** The electrode/electrolyte interphase resistance was calculated by NLLS analysis of the EIS data of panel b-d ($\sum R_i, i = 1, 2, \dots, n$); Table 1 shows the related NLLS results.^[77]

C rate	Cycle life	Equivalent Circuit	χ^2	$\sum R_i (\Omega, i = 1, 2, \dots, n)$
1C	OCV	$R_e(R_1Q_1)(R_2Q_2)(R_3Q_3)Q_g$	9.5×10^{-5}	140 ± 10
1C	1 cycle	$R_e(R_1Q_1)(R_2Q_2)(R_dQ_d)$	8.2×10^{-5}	82 ± 7
1C	200 cycles	$R_e(R_1Q_1)(R_2Q_2)(R_dQ_d)$	3.6×10^{-5}	83 ± 7
1C	500 cycles	$R_e(R_1Q_1)(R_2Q_2)(R_dQ_d)$	2.4×10^{-5}	74 ± 2
2C	OCV	$R_e(R_1Q_1)(R_2Q_2)(R_3Q_3)Q_g$	3.1×10^{-5}	181 ± 7
2C	1 cycle	$R_e(R_1Q_1)(R_2Q_2)(R_dQ_d)$	3.9×10^{-5}	100 ± 20
2C	200 cycles	$R_e(R_1Q_1)(R_2Q_2)(R_dQ_d)$	2.6×10^{-5}	78 ± 6
2C	500 cycles	$R_e(R_1Q_1)(R_2Q_2)(R_dQ_d)$	2.6×10^{-5}	90 ± 10
5C	OCV	$R_e(R_1Q_1)(R_2Q_2)(R_3Q_3)Q_g$	7.1×10^{-5}	110 ± 10
5C	1 cycle	$R_e(R_1Q_1)(R_2Q_2)(R_dQ_d)$	1.3×10^{-4}	70 ± 10
5C	200 cycles	$R_e(R_1Q_1)(R_2Q_2)(R_3Q_3)(R_dQ_d)$	9.8×10^{-6}	80 ± 10
5C	500 cycles	$R_e(R_1Q_1)(R_2Q_2)(R_dQ_d)$	6.4×10^{-5}	77 ± 4

Table 1

Salt 01	Salt 02	Solvent	Acronym
LiFSI; 1 mol kg ⁻¹	LiNO ₃ ; 0.4 mol kg ⁻¹	Diethylene glycol dimethyl ether (DEGDME)	(A) LiFSI-LiNO ₃ -DEGDME
LiTFSI; 1 mol kg ⁻¹	LiNO ₃ ; 0.4 mol kg ⁻¹	Diethylene glycol dimethyl ether (DEGDME)	(B) LiTFSI-LiNO ₃ -DEGDME
LiBETI; 1 mol kg ⁻¹	LiNO ₃ ; 0.4 mol kg ⁻¹	Diethylene glycol dimethyl ether (DEGDME)	(C) LiBETI-LiNO ₃ -DEGDME
LiFSI; 1 mol kg ⁻¹	LiNO ₃ ; 0.4 mol kg ⁻¹	Triethylene glycol dimethyl ether (TREGDME)	(D) LiFSI-LiNO ₃ -TREGDME
LiTFSI; 1 mol kg ⁻¹	LiNO ₃ ; 0.4 mol kg ⁻¹	Triethylene glycol dimethyl ether (TREGDME)	(E) LiTFSI-LiNO ₃ -TREGDME
LiBETI; 1 mol kg ⁻¹	LiNO ₃ ; 0.4 mol kg ⁻¹	Triethylene glycol dimethyl ether (TREGDME)	(F) LiBETI-LiNO ₃ -TREGDME

Table 2

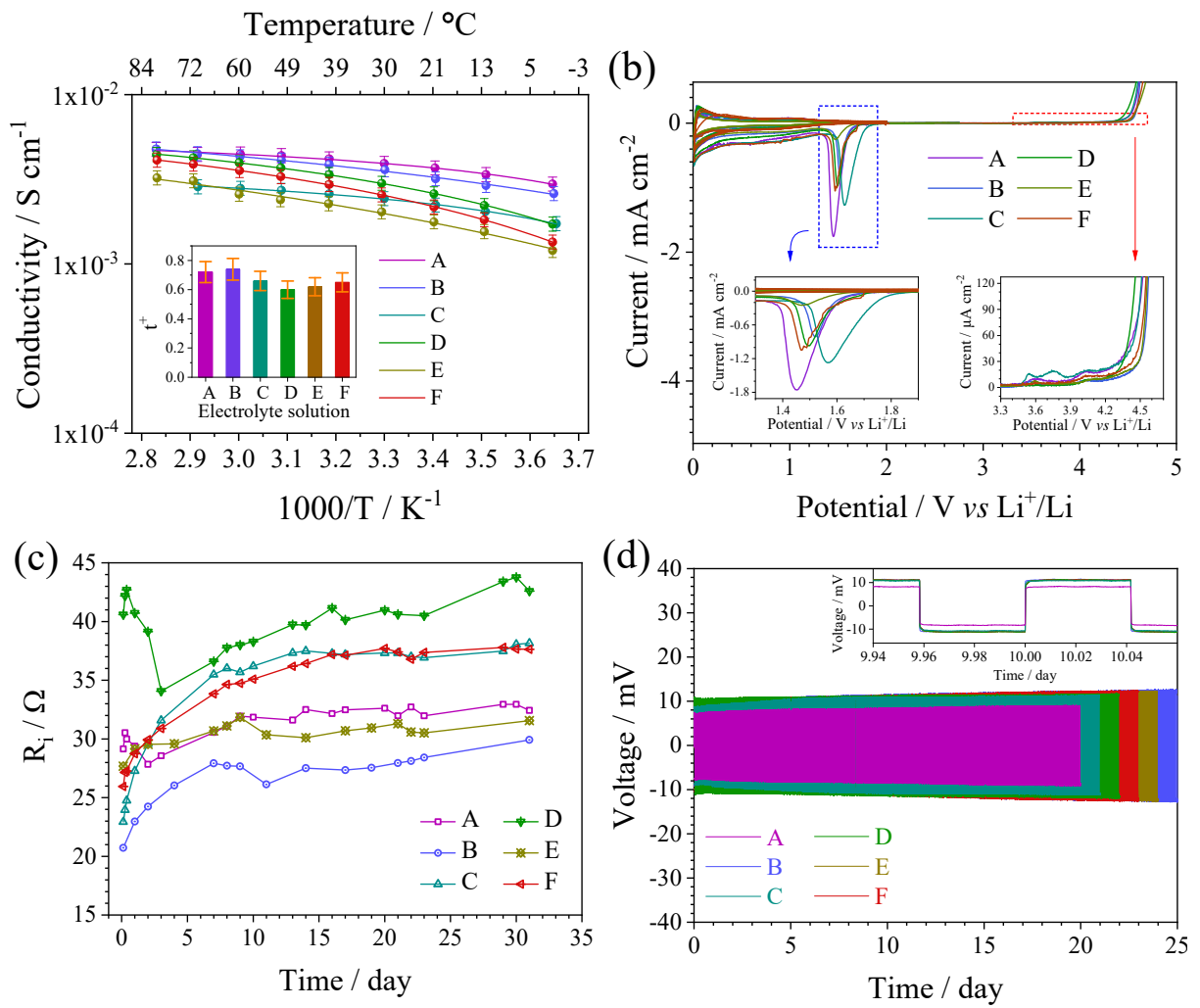


Figure 1

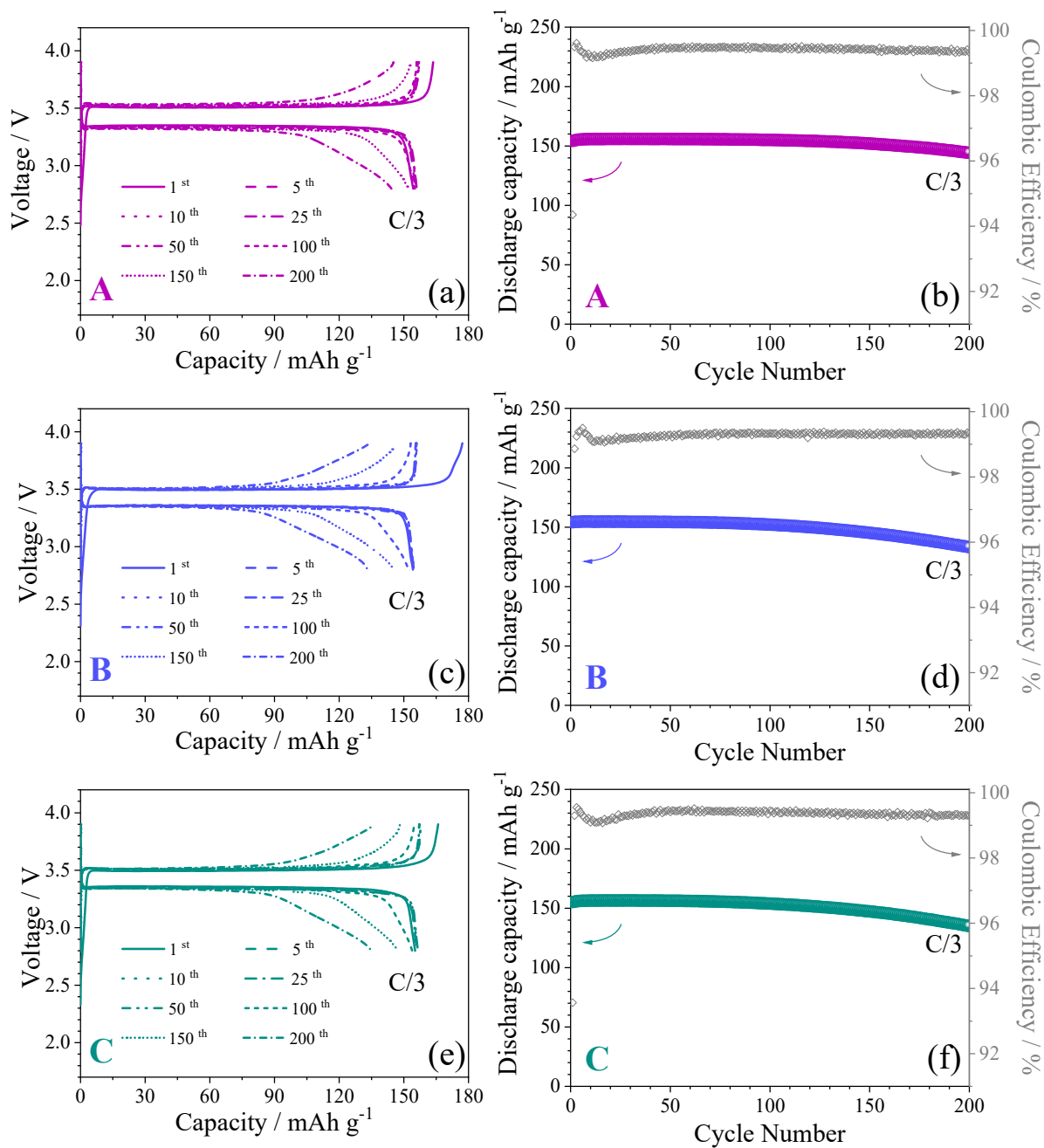


Figure 2

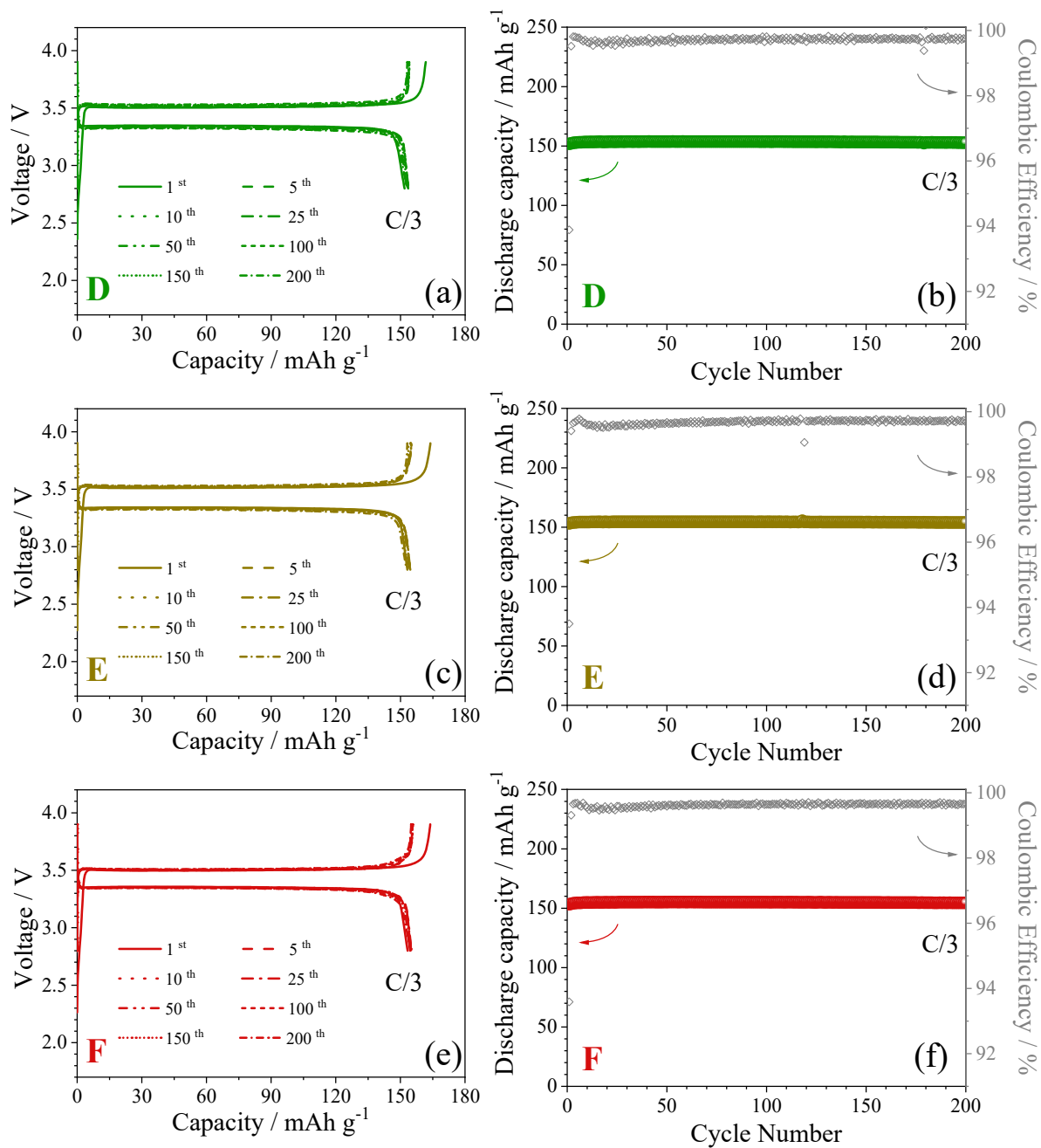


Figure 3

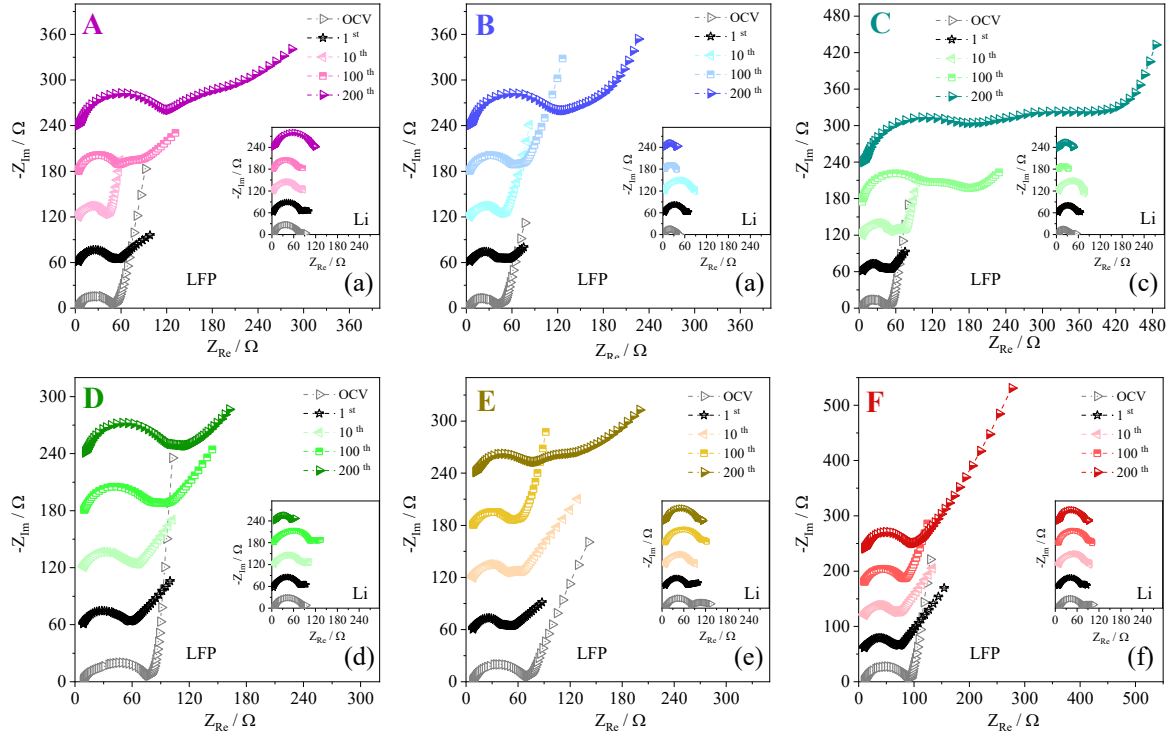


Figure 4

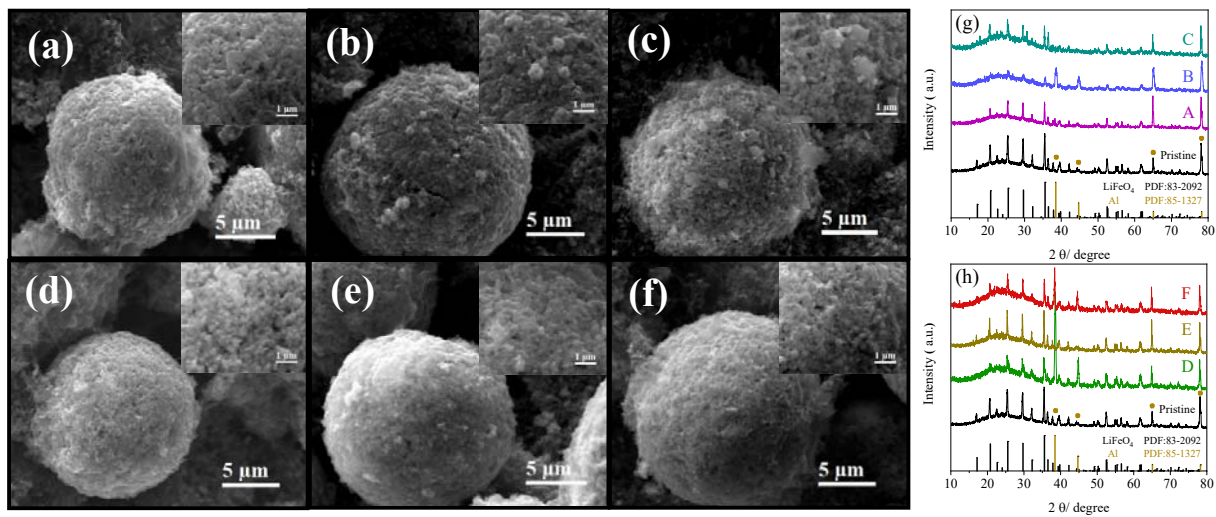


Figure 5

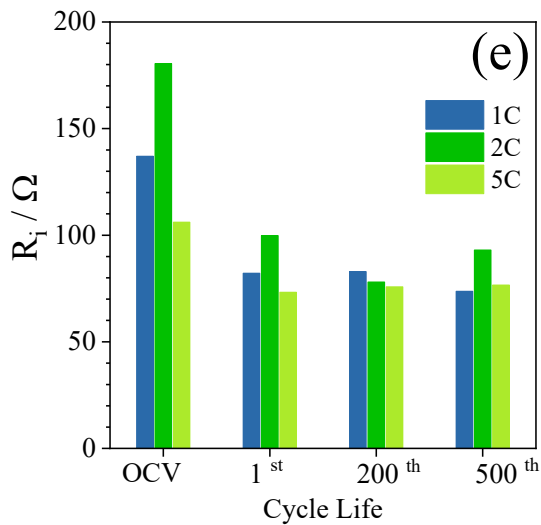
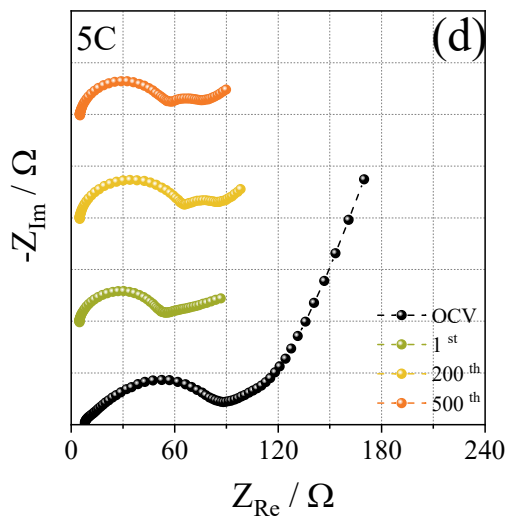
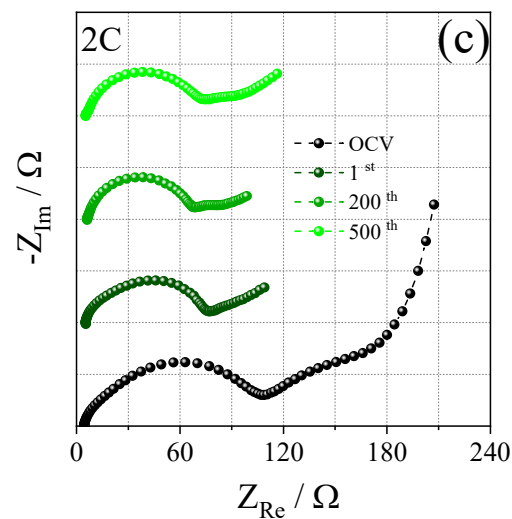
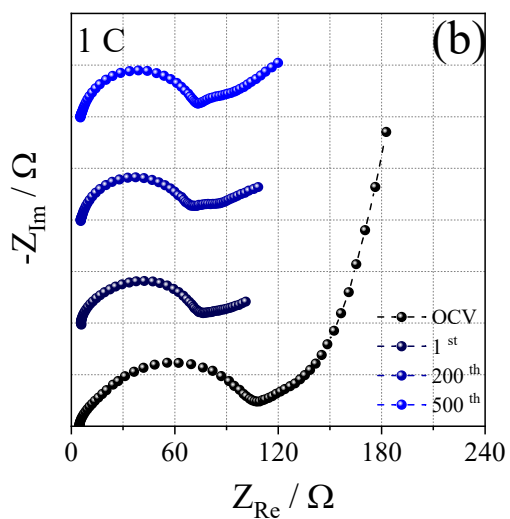
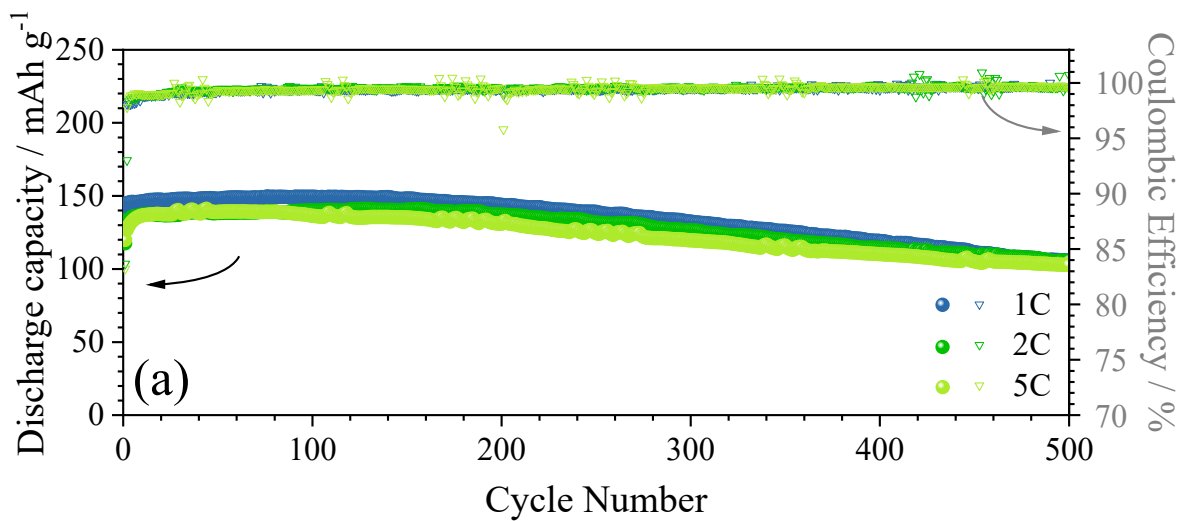
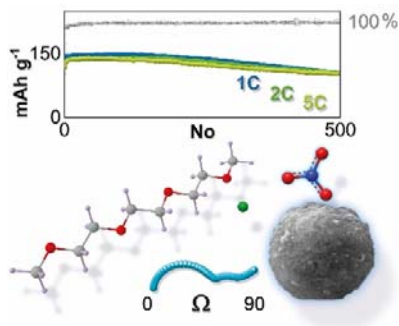


Figure 6

Table of contents



Possible solution! Triglyme and diglyme enhanced by LiNO₃ ensure highly performing lithium-metal batteries benefiting from stable electrode/electrolyte interphases. The glyme-based solutions exhibit a suitable ionic transport, a wide electrochemical stability window, a favorable anode passivation, and LiFePO₄/electrolyte behavior depending on the solvent chemistry. Li/LiFePO₄ cells deliver a capacity from 140 to 150 mAh g_{cathode}⁻¹ within the current range between 5C and 1C, with a retention higher than 70% after 500 cycles and a coulombic efficiency approaching 100%.